

Computational Probabilistic Quantification of Pro-arrhythmic Risk from Scar and Left-to-Right Heterogeneity in the Human Ventricles

Mikael Wallman^{1,2}, Alfonso Bueno-Orovio³, Blanca Rodriguez¹

¹ Department of Computer Science, University of Oxford, Oxford, UK

² Fraunhofer-Chalmers Centre, Göteborg, Sweden

³ Oxford Centre for Collaborative Applied Mathematics, University of Oxford, Oxford, UK

Abstract

Both scar and left-to-right ventricular (LV/RV) differences in repolarization properties have been implicated as risk factors for lethal arrhythmias. As a possible mechanism for the initiation of re-entry, a recent study has indicated that LV/RV heterogeneities in the adaptation of action potential duration (APD) to changes in heart rate can cause a transient increase in APD dispersion following rate acceleration, promoting unidirectional block of conduction at the LV/RV junction. In the presence of an ischemic region and ectopic stimulation, a pathological dispersion in repolarization has been suggested to increase the risk of electrical re-entry. However, the exact location and timing of the ectopic activation play a crucial role in initiation of re-entry, and certain combinations may lead to re-entry even under normal LV/RV dispersion in repolarization. This suggests that the phenomenon needs to be investigated in a probabilistic way. In this study we employ a computationally efficient, phenomenological model to quantify the pro-arrhythmic effects associated with a range of combinations of position and timing of an ectopic activation. This allows us to probabilistically study how increasing interventricular dispersion of repolarization increases arrhythmic risk. Results indicate that a larger LV/RV dispersion more than doubles the length of the time window during which the ventricles are vulnerable to re-entry, and leads to a four-fold increase in the probability of re-entry within the vulnerable window.

1. Introduction

Ventricular heterogeneity in repolarization is one of the most important contributors to the electrophysiological substrate leading to the occurrence of lethal arrhythmias such as ventricular fibrillation [1]. A number of studies have demonstrated the complex spatio-temporal mechanisms that modulate ventricular heterogeneity in repolarization and pro-arrhythmic risk. Ventricular heterogeneity

in repolarization and arrhythmic risk are known to increase with sudden changes in rate [2, 3], due to the highly rate-dependent properties of the APD. The dynamics of APD adaptation underlie the adaptation of the QT interval in the electrocardiogram. Importantly, patients with protracted QT interval rate adaptation appear to have an increased arrhythmic risk [4], highlighting the importance of ventricular rate adaptation dynamics in arrhythmogenesis. A recent computational study based on *in vivo* human data has suggested a mechanism of reentry initiation from increased dispersion of APD adaptation in the presence of ischemia [5].

The aim of this study is to investigate the pro-arrhythmic effects of LV/RV differences in APD adaptation using computer simulations. Specifically, we aim to provide a quantitative characterization of the role of interventricular dispersion of repolarization in arrhythmogenesis, within a range of times and positions for the initiation of ectopicity. In order to achieve this, we develop a fast phenomenological model, able to reproduce the essential mechanisms involved in APD adaptation and the initiation of re-entry. Using an image-derived human ventricular model, we then compare two scenarios: one with normal difference in LV/RV rate adaptation, and another with slow, pathological, LV rate adaptation, leading to a larger dispersion in LV/RV repolarization.

2. Methods

2.1. Anatomical model

The anatomical model used for this study is a human ventricular mesh derived from computed tomography data [6], incorporating 55000 nodes. The model includes an algorithmically defined fibre orientation derived from experimental data [7], generated using the Chaste simulation package [8, 9]. As an aid for assigning specific properties to the respective ventricles, each node of the model was given a value between 0 and 1, with values close to zero

signifying LV specific properties and values close to 1 signifying specific RV properties, based on their distance to the LV and RV endocardium respectively. Additionally, a non-conductive spherical volume centered around the septum was included in the model, roughly mimicking an infarcted region resulting from LAD occlusion. Finally, a volume close to the scar, near the base of the RV, was assigned as the origin of ectopic beats, emulating the ectopic activity often observed in the peri-infarct zone. The anatomical model is shown in Fig. 1, along with color coding for the LV and RV properties, and the non-conductive and ectopic regions marked with the labels SCAR and STIM, respectively.

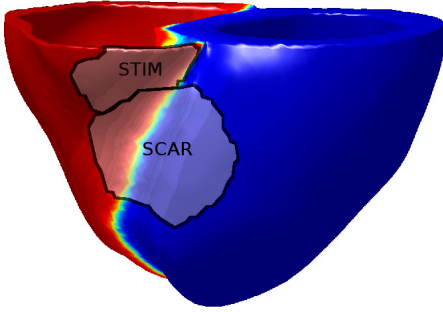


Figure 1. Computational anatomical model. Blue and red respectively signify LV and RV specific properties. The region marked SCAR is non-conductive, whereas STIM indicates the region of applied ectopic activity.

2.2. Conduction model

To describe the electrical conduction properties of the model, we used the graph method developed in [10]. Briefly, the method relies on describing the cardiac tissue as a connected graph, where every edge is associated with a traveling cost. By finding the fastest path through the graph between pairs of nodes, activation times can be obtained with minimal computational cost. The costs $c_{i,j}$ associated with traveling along a graph edge connecting two nodes i and j are calculated according to

$$c_{i,j} = \sqrt{v(n_i, n_j)^T D_{i,j}^{-1} v(n_i, n_j)} / F, \quad (1)$$

where $v(n_i, n_j)$ is the vector going from node i to node j , F is a speed function, and $D_{i,j}$ is a tensor describing the anisotropy resulting from the cell orientation between nodes i and j . The conduction paths in the model were computed using a modified version of Dijkstra's algorithm that will be described in Section 2.4.

2.3. Action potential model

The dynamics governing the adaptation of the action potential duration, A , within the model are described using

the following recurrence relation for each node, following the approach presented in [11]:

$$A_{n+1} = [1 - \alpha e^{-D_n/\tau_2}] G(D_n) + [\alpha - 1 + \frac{A_n}{G(D_{n-1})} e^{-(A_n+D_n)/\tau_2}] G(D_n), \quad (2)$$

$$G(D_n) = a_1 - a_2 e^{-D_n/\tau_1}. \quad (3)$$

Here, n is an index counting the number of action potential and D is the diastolic interval. The values for the parameters in Eqs. (2) and (3) were: $a_{1,LV} = 404$, $a_{2,LV} = 197$, $\tau_{1,LV} = 77$, $\tau_{2,LV} = 76927$, $\alpha_{LV} = 1.05$ and $a_{1,RV} = 358$, $a_{2,RV} = 121$, $\tau_{1,RV} = 97$, $\tau_{2,RV} = 49399$ and $\alpha_{RV} = 1.08$ for LV and RV as indicated, and with $\tau_{2,LV} = 128720$ for the slower adaptation. These values were adapted to data presented in [5], using the Nelder-Mead optimization scheme as implemented in MATLAB. Figure 2 shows the dynamics of the APD dispersion resulting from the normal (solid line) and slow LV adaptation properties (dashed line), respectively, after a change of pacing interval from 750 ms to 400 ms.

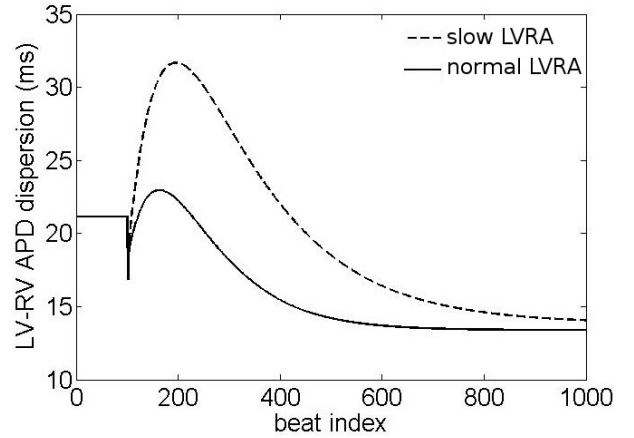


Figure 2. LV/RV dispersion in APD, following an abrupt change in pacing rate from 750 to 400 ms. Change in pacing rate occurs at beat 100. Data is shown for normal (solid line) and slow (dashed line) LV rate adaptation (LVRA).

2.4. Activation and repolarization times

Based on the graph based method described in Section 2.2 and the model of APD adaptation described in Section 2.3, we now describe how the activation and repolarization at the tissue level are computed. The algorithm is similar to the well known Dijkstra's algorithm [12], but is modified to take repolarization into account, allowing nodes to be activated several times and thus allowing simulation of re-entrant activation. This modification is roughly analogous to that presented for the fast marching method in [13].

Briefly, the algorithm works by using a priority queue Q to keep track of the order in which to expand nodes n to maintain a causal flow of information. In this context, expanding a node means finding its neighbors n_i , and calculating their arrival time $t(n_i)$, using information propagated from node n . The value of $t(n)$ is used to determine the position of a node n in Q . When a node is pulled from the queue, its APD is calculated according to Eq. (2). For a start node n_0 , a pseudo-code description of the algorithm can be found in Algorithm 1.

Algorithm 1 Modified Dijkstra's Algorithm

```

 $Q \leftarrow Q \cup n_0$ 
 $t(n_0) \leftarrow 0$ 
while  $Q \neq \emptyset$  do
 $n \leftarrow \operatorname{argmin}_{n \in Q} t(n)$ 
 $Q \leftarrow Q \setminus n$ 
 $APD(n) \leftarrow F(APD(n), DI_1(n), DI_0(n))$ 
 $time \leftarrow t(n)$ 
for all  $n_i \in \text{NEIGHBORS}(n)$  do
if  $t(n_i) + APD(n_i) < time + \text{COST}(n, n_i)$  then
 $t(n_i) \leftarrow t(n) + \text{COST}(n, n_i)$ 
 $Q \leftarrow Q \cup n_i$ 
end if
end for
end while

```

2.5. Initiation of re-entry

The model was periodically activated from the bottom of both ventricles with a pacing interval of 750 ms until the APD distribution remained unchanged, followed by a change in pacing interval to 400 ms until the maximal dispersion in repolarization was reached after approximately 100 beats as shown in Fig. 2. Finally, reentry was initiated using an ectopic stimulus at the basal side of the non-conductive zone, inside the region marked STIM in Fig. 1.

Rather than keeping the timing and placement of the ectopic stimulus fixed, a range of different combinations within the STIM region were investigated. The times were varied between 265 ms and 295 ms in 10 steps, and 843 different positions were investigated, resulting in a set of 8430 possible combinations. This was done for both the normal and slow adaptation parameters as described in Section 2.3, resulting in a total of 16860 simulated scenarios.

3. Results

Two sets of 8430 simulations were performed, corresponding to the normal and slow LV APD adaptation, as described in the previous section. An individual simulation took of the order of 100 ms to compute, often leading

to CPU times faster than real time. For some combinations of position and timing of the ectopic beat, unidirectional block on the still-repolarizing LV side initiated a counter-clockwise reentry around the central conduction block as depicted in Fig. 3.

For each of the investigated timings of the ectopic stimulus, the percentage of positions within the STIM region of the ectopic stimulus that lead to re-entry was recorded. These results are visualized in Fig. 4. As can be observed from the figure, the larger dispersion of repolarization lead to a marked increase in the probability of re-entry, as well as an extension of the range of timings of the ectopic beat which lead to re-entry. An ectopic beat at approximately 282 ms after last intrinsic activation appears to lead to the highest incidence of re-entry. At this time, the increased interventricular dispersion of repolarization lead to an approximately four-fold increase in the number of positions for the ectopic beat that lead to re-entry.

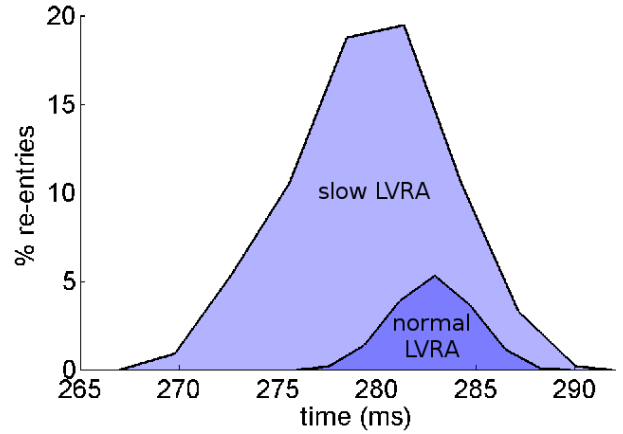


Figure 4. Percentage of resulting sustained ventricular re-entries depending on ectopic timing since last intrinsic activation, for multiple ectopic locations close to the infarcted area. The upper curve corresponds to the slow LV rate adaptation (LVRA) of APD, while the lower curve corresponds to the normal LV APD adaptation.

4. Discussion

In this work, we have presented a method for simulating re-entry with minimal computational costs. The new method has enabled us to investigate the effects of interventricular dispersion of repolarization on the risk initiation of re-entry. In order to quantify the risk, a range of possible locations and timings were investigated, comprising a total of over 16000 simulated scenarios. This has allowed the quantification of the arrhythmic risk within the investigated range. Results show that the slow LV rate adaptation more than doubles the length of the vulnerable time window, and leads to a four-fold increase in the prob-

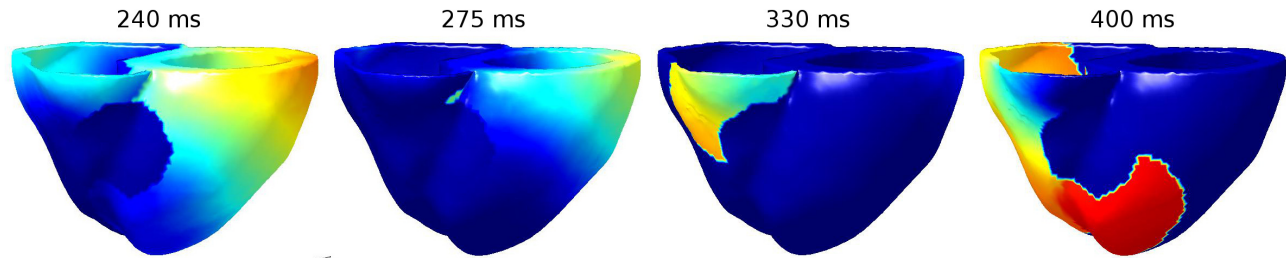


Figure 3. Electrical reentry following ectopic stimulation at 275 ms after last intrinsic activation. Unidirectional conduction block is caused by the slower APD rate adaptation of the LV, which is still repolarizing at the time of the ectopic stimulus. The four panels show the pseudo-potential of the tissue at 240, 275, 330 and 400 ms, for the left, middle left, middle right and right panels, respectively.

ability of re-entry within the window.

The employed graph based model provides a simplified representation of the dynamical properties of cardiac tissue. Although capturing essential characteristics of APD restitution and adaptation, it does not currently take into account effects from CV restitution and adaptation. The incorporation of such effects forms an interesting topic for future developments of the presented methods. Additional planned improvements include a more detailed model of the infarcted region, as well as investigation of a larger range of tissue rate adaptation and restitution properties.

Acknowledgements

ABO was supported by Award No. KUK-C1-013-04, made by King Abdullah University of Science and Technology (KAUST). BR holds Medical Research Council Career Development, Industrial Partnership and Centenary Awards.

References

- [1] Nash MP, Bradley CP, Sutton PM, Clayton RH, Kallis P, Hayward MP, Paterson DJ, Taggart P. Whole heart action potential duration restitution properties in cardiac patients: a combined clinical and modelling study. *Exp Physiol* 2006; 91(2):339–354.
- [2] Kop WJ, Verdino RJ, Gottdiener JS, O’Leary ST, Bairey Merz CN, Krantz DS. Changes in heart rate and heart rate variability before ambulatory ischemic events(1). *J Am Coll Cardiol* 2001;38(3):742–749.
- [3] Eisenberg SJ, Scheinman MM, Dullet NK, Finkbeiner WE, Griffin JC, Eldar M, Franz MR, Gonzalez R, Kadish AH, Lesh MD. Sudden cardiac death and polymorphous ventricular tachycardia in patients with normal QT intervals and normal systolic cardiac function. *Am J Cardiol* 1995; 75(10):687–692.
- [4] Pueyo E, Husti Z, Hornyik T, Baczk I, Laguna P, Varró A, Rodríguez B. Mechanisms of ventricular rate adaptation as a predictor of arrhythmic risk. *Am J Physiol Heart Circ Physiol* 2010;298(5):H1577–1587.
- [5] Bueno-Orovio A, Hanson BM, Gill JS, Taggart P, Rodriguez B. In vivo human left-to-right ventricular differences in rate adaptation transiently increase pro-arrhythmic risk following rate acceleration. *PLoS ONE* 2012; 7(12):e52234.
- [6] Bernabeu M, Wallman M, Rodriguez B. Shock-induced arrhythmogenesis in a human model with patient-specific anatomy. *Heart Rhythm* 2010;2010.
- [7] Potse M, Dube B, Richer J, Vinet A, Gulrajani RM. A comparison of monodomain and bidomain reaction-diffusion models for action potential propagation in the human heart. *IEEE Trans Biomed Eng* 2006;53(12):2425–2435.
- [8] Bernabeu M, Bishop M, Pitt-Francis J, Gavaghan D, Grau V, Rodriguez B. High performance computer simulations for the study of biological function in 3D heart models incorporating fibre orientation and realistic geometry at paracellular resolution. In *Computers in Cardiology*, 2008. 2008; 721–724.
- [9] Pitt-Francis J, Pathmanathan P, Bernabeu MO, Bordas R, Cooper J, Fletcher AG, Mirams GR, Murray P, Osborne JM, Walter A, et al. Chaste: a test-driven approach to software development for biological modelling. *Comp Phys Comm* 2009;180(12):2452–2471.
- [10] Wallman M, Smith NP, Rodriguez B. A comparative study of graph-based, eikonal, and monodomain simulations for the estimation of cardiac activation times. *IEEE Trans Biomed Eng* 2012;59(6):1739–1748.
- [11] Kalb SS, Tolkacheva EG, Schaeffer DG, Gauthier DJ, Krasowska W. Restitution in mapping models with an arbitrary amount of memory. *Chaos* 2005;15(2):023701.
- [12] Dijkstra EW. A note on two problems in connexion with graphs. *Numerische Mathematik* 1959;1:269–271.
- [13] Pernod E, Sermesant M, Konukoglu E, Relan J, Delingette H, Ayache N. A multi-front eikonal model of cardiac electrophysiology for interactive simulation of radio-frequency ablation. *Computers and Graphics* 2011;35:431–440.

Address for correspondence:

Mikael Wallman
 Department of Computer Science, University of Oxford
 Parks Rd, Oxford OX1 3QD, UK
 mikw@cs.ox.ac.uk